Chapter 2

Acetone Oxidation Using Ozone on Manganese Oxide Catalysts

2.1 Introduction

This chapter presents an activity study of VOC oxidation using ozone over supported manganese oxide catalysts. The VOC used in this study was acetone, which is a common solvent used in many industrial processes such as surface coating, painting, and extraction. Similar to other VOCs, acetone is harmful to human health. Acetone has been studied in the literature as an example of a VOC containing a carbonyl group [1, 2, 3, 4]. In one of the studies involving manganese oxide as the catalyst, Baldi et al. [5] found that the conversion of acetone with excess oxygen over Mn_3O_4 started at near 473 K, with acetaldehyde being the main product, together with minor amounts of acetic acid. The conversion increased to high values in the temperature range of 510-563 K where the only carbon-containing product was CO_2. In another study by Parida and Samal [2] manganese nodules collected from the Indian Ocean were used as the catalysts in the combustion with oxygen of VOCs, including acetone, and it was found that complete oxidation of acetone over these nodules was achieved at a temperature less than 573 K. It was reported by Ragaini et al. [3] that the oxidation temperature of acetone decreased by 10 % when ozone was used in the reaction compared to oxygen using a barium promoted copper-chromite catalyst.

In this study the manganese oxide active phase was placed on alumina foam substrates. These are porous monolithic materials with low densities and novel physical, mechanical, and thermal properties that offer potential application as catalyst supports [6, 7, 8, 9]. Dhandapani et al. [10] compared the pressure drop in pellets, monoliths, and foams with the same constant geometric surface area of 620 cm^2 and found that the monolith and foam had a similar gas resistance which was much smaller than that of the pellets. They also compared the catalytic performance between a straight pore monolith and a foam and found that there was little difference between the two substrates, suggesting that the foam can be employed instead of the commonly used monolith. Patcas [11] studied the methanol-to-olefins conversion over zeolite-coated ceramic foams and found that the use of the foams as carriers allowed variation of the catalyst bulk thickness with almost no influence on the hydrodynamics, and at the same time provided high turbulence and radial mixing.

This chapter reports a comparative study of the activities of silica- and alumina-supported manganese oxide catalysts deposited on foam substrates for the oxidation of acetone. The use of ozone resulted in a significant reduction in the reaction temperature and increase in reaction rate.

2.2 Experimental

2.2.1 Catalyst preparation

The substrate material for the catalyst was a monolithic aluminum oxide foam (Amporex, Fiber-Ceramics, Inc., Cincinnati, Ohio) cut into cylindrical shape of 3.5 cm diameter and 1.3 cm height and approximately 20 g in weight. The original pore density of the foam was a nominal 30 pores per inch (ppi). The catalysts (10 wt % MnO_x/SiO_2 and 10 wt % MnO_x/Al_2O_3) were

prepared by a multiple impregnation method. The foam substrates were first washcoated with SiO_2 (Cabot, Cabosil LM130, 134 m^2 g^{-1}) and Al_2O_3 (Degussa Aluminumoxid C, 96 m^2 g^{-1}) powders. A slurry of 18.0 g silica in 150 ml water and a slurry of 15.3 g alumina in 100 ml water were prepared for the impregnation of the foam substrates. The foams were placed in the slurry solutions for approximately 30 seconds, removed, and then were shaken to remove as much residual liquid as possible. The coated samples were dried at 393 K for 6 h and calcined at 773 K for 8 h in an oven. During the heating cycles, air was introduced through a 1/8″ tube pointing toward the oven floor in the middle of the oven to provide good circulation. Three or more coating/heating cycles were used to get the washcoated sample. The amount of washcoat was obtained from the gain in weight of the original foam by application of the washcoat, and typically was about 2.0-4.0 g (1-2 %) for alumina and 1.5-2.0 g (0.7-1 %) for silica. Finally the coated foams were impregnated with an aqueous solution of the precursor manganese (II) acetate tetrahydrate (Aldrich, 99.99 %). The samples were dipped into the solution quickly, shaken to remove the excess solution, and then dried at 393 K for 6 h and calcined at 773 K for 8 h. The impregnation solution was not completely utilized, but it was found that using a two-fold excess of the manganese precursor (5.1 g and 2.5 g of manganese acetate, respectively for alumina and silica in 200 cm^3 of water) gave approximately 10 wt % of MnO_2 based on the weight of the two washcoats. The air jet was again used during the drying/calcining process to ensure even drying. Typical weights of the original foams, washcoats, and the final loadings based on the washcoats are presented in Table 2-1.

Table 2-1. Sample weight summary for each step in the foam catalyst preparation.

Catalyst samples	Weight Blank foam g	Weight Washcoated sample g	Weight Washcoat g	Weight Total g	Weight MnO_x g	wt % MnO_x (Washcoat)
10 wt% MnO_x/SiO_2	20.123	21.975	1.852	22.190	0.215	10.4
10 wt% MnO_x/Al_2O_3	23.308	23.308	4.294	23.820	0.512	10.7
Si coated foam	19.083	20.628	1.545	-	-	-
Al coated foam	19.968	22.167	2.199	-	-	-

Another 10 wt % manganese oxide on silica catalyst was prepared for the Raman spectroscopy experiments by the incipient wetness impregnation method using an aqueous solution of manganese acetate (Aldrich, 99.99 %) added dropwise to a previously calcined (773 K for 6 h) support, SiO_2 (Cabot, Cabosil EH-5, 320 m^2/g). After impregnation, the sample was dried at 393 K for 6 h and then was calcined at 773 K for 6 h at a heating rate of 0.83 K/s (5 K/min). This sample was denoted 10 wt % MnO_x/SiO_2-H to indicate that it was prepared on a higher surface area silica, and to distinguish it from the sample obtained on the foam substrate.

2.2.2 Catalyst characterization

The foam samples were crushed and ground to fine powders for BET, temperature-programmed reduction (TPR), and oxygen chemisorption measurements. For other analyses, the washcoat containing the supported manganese oxide was knocked off the foam structure and ground into fine powders.

X-ray diffraction (XRD) patterns were obtained with an ASC-0007 model diffractometer using Cu Kα radiation generated at 45 kV and 40 mA. The measurements were obtained at a 2θ angle range of 10º to 90º using a scanning rate of 0.03º/s (2º/min).

Extended x-ray absorption fine structure (EXAFS) spectroscopy measurements were carried out in transmission mode at the X18B beam line of the NSLS (National Synchrotron Light Source) with a 2.5 GeV ring energy and 300-400 mA ring current. The beam line used a Si (111) crystal monochromator and gave an energy resolution of 2 eV. WinXas 2.3 software was used to analyze the EXAFS results. Amounts of 0.5 g of the samples were pretreated in a 20 % oxygen/helium mixture at 723 K for 3 h and then transferred into cells with Kapton windows without exposure to the atmosphere.

Temperature-programmed reduction (TPR) and oxygen chemisorption measurements were carried out in a standard flow system equipped with a computer interfaced mass spectrometer (Dycor/Ametek Model MA 100). Quantities of 0.2 g of catalysts were used in the experiments.

For the TPR measurements the catalysts were pretreated at 773 K for 2 h in 54 μmol/s (80 cm^3/min) of oxygen (Air Products, > 99.6 %) flow to remove excess moisture and carbon impurities. Then the catalyst sample was reduced in 68 μmol/s (100 cm^3/min) of hydrogen (Air products, > 99.6 %) flow from room temperature to 1073 K at a rate of 0.03 K/s (2 K/min). The mass spectrometer signal of H_2O^+ (m/e = 18) was monitored during the reduction process to determine the reduction temperature, (T_{red}), which was taken to be the temperature right before the onset of bulk reduction. Experimentally, this was the point at which the signal increased dramatically in the TPR trace. Oxygen chemisorption was performed at this reduction temperature.

The procedure for oxygen chemisorption involved pretreatment of the catalyst at 773 K for 2 h in 54 μmol/s (80 cm^3/min) of oxygen (Air products, > 99.6 %) followed by reduction of the sample in 68 μmol/s (100 cm^3/min) of hydrogen (Air products, > 99.6 %) at T_{red} for 2 h.

After reduction the flow was switched to 68 µmol/s (100 cm^3/min) of helium (Air products, > 99.6 %) at the same temperature and pulses (19.56 µmol) of oxygen were injected into the reactor while monitoring the intensity of the O_2^+ signal. The injection of oxygen was continued until equal oxygen peak areas were obtained, indicating saturation of the sample surface. The total amount of oxygen adsorbed was determined by the difference between the area of the saturated peaks and the area of the peaks before saturation. The oxygen uptake value was estimated by

$$\text{Oxygen Uptake (µmol/g)} = \frac{19.56 \mu mol}{m} \sum_i \left(\frac{A_{sat} - A_i}{A_{sat}} \right), \quad (1)$$

where m is the mass of the catalyst sample (g), A_{sat} is the oxygen peak area at saturation and A_i is the area of the oxygen peaks before saturation. Dispersion was calculated based on the amount of atomic oxygen uptake and the total amount of manganese loaded on the sample.

Brunauer-Emmett-Teller (BET) surface area measurements were carried out in an automatic volumetric adsorption apparatus (Micromeritics, ASAP 2010) using amounts of 0.2 g of samples loaded into a quartz reactor and degassed at 423 K in vacuum prior to measurement. A five-point N_2 (Air products, > 99.6 %) analysis method was used to determine the surface area of each sample.

2.2.3 Reactivity measurements

The acetone oxidation reaction was carried out in a flow reactor system (Figure 2-1) using a 3.5 cm ID tubular fixed-bed quartz reactor at atmospheric pressure. The cylindrical foam catalysts (7.314 g of 10 wt % MnO_x/SiO_2 and 6.738 g of 10 wt % MnO_x/Al_2O_3) were wedged

into the middle of the tube with quartz tape to prevent gas bypass. The volumes below and above the catalysts were packed with glass spheres to minimize the residence time of the gas in the empty reactor space and to achieve efficient preheating of the reactants. The pressure drop across the sample was measured with a digital pressure gauge (Mensor, DPG II, Model 15000) with switchable inlets before and after the reactor. The main flow stream was air, purified by passage through a Balston filter (Whatman Inc., Model 912). The air stream was drawn through the system by a compressor (Shizoki, Japan, Model WME-RS) located at the exit of the system, and the total flow rate was measured by a flow meter (Top Track, Series 820) and controlled by a variable autotransformer (Staco Energy Products Co., Dayton, OH, Type 3PN1010) connected to the compressor. Ozone was produced by passing oxygen (Air products, > 99.6 %) through a corona discharge in a high voltage ozone generator (OREC, V5-0) and was introduced in an independent line. The ozone concentration was monitored via an ozone monitor (In USA, Model H1) with a UV lamp detector. Acetone was introduced through another independent line using a two-stage bubbler placed inside an ice bath with a temperature of 273 K. The overall acetone concentration was 0.10 mol % (1,000 ppm) and was set by regulating the air (Air Products, > 99.6 %) flow through the bubbler with a mass flow controller. The acetone vapor pressure (9.25 kPa) was calculated from Antoine's equation

$$y_v = \frac{P_v}{P_{tot}} = \frac{10^{\left(A - \frac{B}{T+C}\right)}}{P_{tot}}, \qquad (2)$$

where P_v and P_{tot} are the vapor pressure and total pressure in units of torr; T is temperature in units of ºC; y_v is the partial vapor pressure fraction; and A, B, and C are the Antoine coefficients for acetone with values equal to 7.02447, 1161, and 224, respectively.

A gas chromatograph (GC) (HP 5890A) equipped with a flame ionization detector with a Chrom W-AW 80/100 column (Alltech, 6′ × 1/8″ × 0.085″ SS) and a thermal conductivity detector with a Hayesep A 80/100 packed column (Alltech, 36′ × 1/8″ × 0.085″ AT-Steel) was used to measure the concentration of the acetone, CO, and CO_2. The GC was capable of detecting other organic compounds such as acetic acid, acetaldehyde, methanol, methane, ethane, ethylene, and acetylene. Importantly, in the catalytic testing, points were taken at increasing and decreasing temperatures to establish catalyst stability. Measurements were taken after 30 min to establish steady-state.

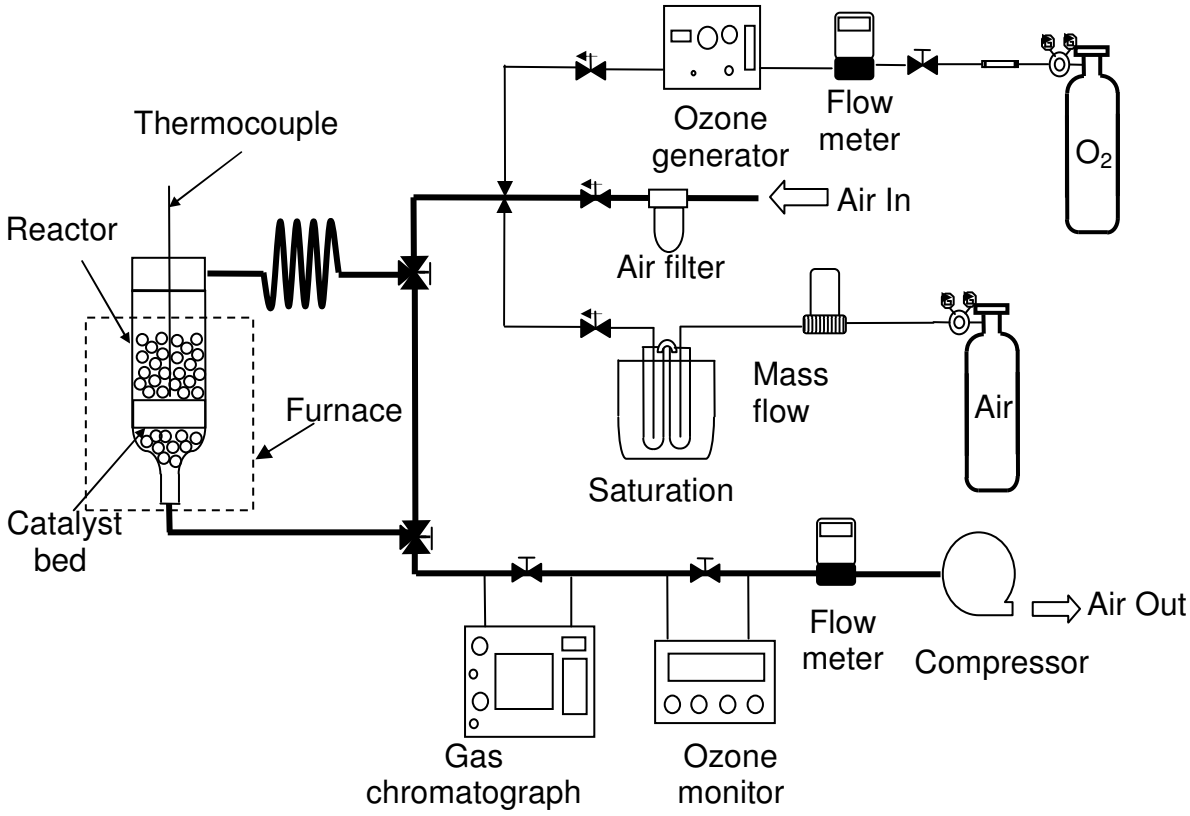

Figure 2-1. Schematic for acetone oxidation reaction system.

2.3.4 Raman spectroscopic measurements

The *in situ* Laser Raman spectroscopy experiments were performed on the powder 10 wt % MnO_x/SiO_2-H catalyst to monitor the adsorbed intermediates resulting from the reaction between acetone and ozone. This work is part of the doctoral dissertation of Corey Reed and is reported here with permission. A schematic of the experimental apparatus is shown in Figure 2-2. The spectroscopic part of the system was made up of an argon ion laser (514.5 nm, Spex Lexel 95) as a light source, a holographic notch filter (Kaiser, Super Notch Plus) to reduce Rayleigh scattering, a single stage monochromator (Spex, 500 M) for the energy dispersion of the light, and a CCD detector (Spex, Spectrum One) for spectral acquisition. The detector slit

width was set at 100 μm giving a resolution of 6 cm^{-1}. The laser was operated at around 160 mW giving a power at the sample of 140 mW.

The powder catalyst sample was pressed into a thin wafer of 0.1 cm thickness and 1.5 cm diameter and was held in place by a stainless steel cap at the end of a ceramic rod. The rod was rotated at 1800 rpm to prevent thermal degradation of the sample by the laser and was enclosed by a synthetic quartz (Suprasil) cell provided with heating tape and inlet and outlet ports, so as to serve as an *in situ* reactor. The catalyst temperature was measured by a thermocouple that was placed in a well 3 mm from the sample. Laser light was focused onto the sample, and the scattered radiation was collected by a lens, filtered, and sent on to the monochromator.

The reactor part of the system was attached to the Raman spectrometer and included a gas delivery system equipped with a two-stage bubbler for the vaporization of liquid acetone. The bubbler was placed inside a refrigerated recirculator (Cole Parmer, Model 1268-14) and was maintained at a temperature of 273 K. The acetone vapor pressure (9.25 kPa) was again calculated from the Antoine equation, and the flow from the bubbler was diluted to achieve the desired acetone concentration. Ozone was again produced via corona discharge by passing pure oxygen through a high voltage ozone generator (OREC, V5-0), and its concentration was measured with an ozone monitor (In USA, Model H1) equipped with a UV lamp detector. A gas chromatograph (GC) (SRI, Model 8610C) equipped with flame ionization and thermal conductivity detectors was used to measure acetone, CO, and CO_2 concentrations. For the GC connected to the spectroscopic system, a 10.0 % AT-1000 80/100 CW-AW (Alltech, 6′ × 1/8″ × 0.086″ AT-Steel) column was connected to the FID and was used for acetone while a Hayesep A 80/100 (Alltech, 36′ × 1/8″ × 0.085″ SS) column was connected to the TCD and was used to separate CO and CO_2.

The sample was pretreated at 723 K for 2 h in an oxygen and helium stream to remove excess moisture and other impurities from the sample. The total flow rate of the feed was 340 μmol/s (500 cm^3/min) giving a space velocity of 170,000 h^{-1}, and was made up of 0.2 mol % (2,000 ppm) acetone, 1.0 mol % (10,000 ppm) ozone, 34 mol % oxygen, and helium as the balance.

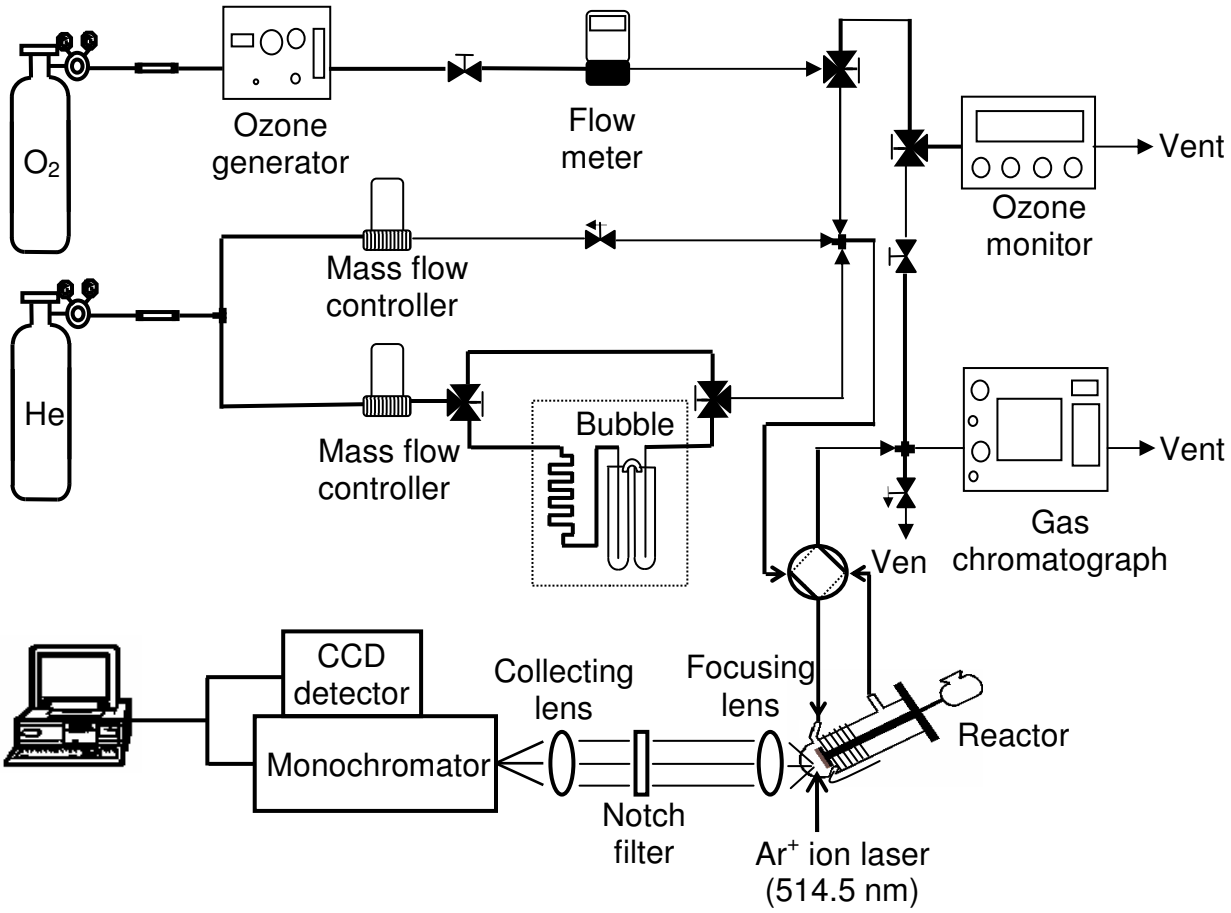

Figure 2-2. Schematic of *in situ* laser Raman spectroscopy system.

2.3 Results

2.3.1 Catalyst characterization result

Figure 2-3 shows the x-ray diffraction results for the catalyst samples, the foam substrates with two different washcoats, the blank foam, and the γ-Al_2O_3. The references α-Al_2O_3 (PDF 10-173), ZrO_2 (PDF 24-1165), Mn_3O_4 (PDF 800382), and β-MnO_2 (PDF 24-0735) are also presented. For both the silica-supported catalyst and the silica washcoated foam there is one broad peak located at around 23º due to amorphous silica. For the alumina-supported catalyst and the alumina washcoated foam there are three broad features at around 36º, 46º, and 66º corresponding to γ-Al_2O_3. For the foam structure, most of the peaks are attributed to α-Al_2O_3, but the other features located at 28º, 32º, 49º, and 52º are due to an additional component, ZrO_2, which is contained inside the foam. The catalyst samples do not show any peaks due to manganese oxides indicating that the supported phase is well dispersed.

Figure 2-4a) shows the Fourier transforms of the Mn K-edge EXAFS spectra for the two catalysts and three references: a) 10 wt % MnO_x/SiO_2; b) 10 wt % MnO_x/Al_2O_3; c) Mn_3O_4; d) Mn_2O_3; and e) MnO_2. The transforms for all the samples have a broad peak at around 0.15 nm corresponding to a Mn-O bond. The transforms of the catalysts, MnO_2, and Mn_3O_4 also have a peak at around 0.25 nm corresponding to a Mn-Mn distance and a broad peak at around 0.32 nm due to contributions from Mn-O and Mn-Mn bonds. The profile of Mn_2O_3 shows a second peak at around 0.28 nm due to contributions from Mn-O and Mn-Mn bonds. Figure 2-4b) shows the corresponding Mn K-edge XANES spectra for the two catalysts and three references. The absorption edge energy (E_0) values for those samples are also displayed in this figure. The E_0 for

the 10 wt % MnO_x/SiO_2 (6.5474 keV) is close to that of the Mn_3O_4 (6.5467 keV), and the E_0 for the 10 wt % MnO_x/Al_2O_3 (6.5484 keV) is close to that of the Mn_2O_3 (6.5479 keV).

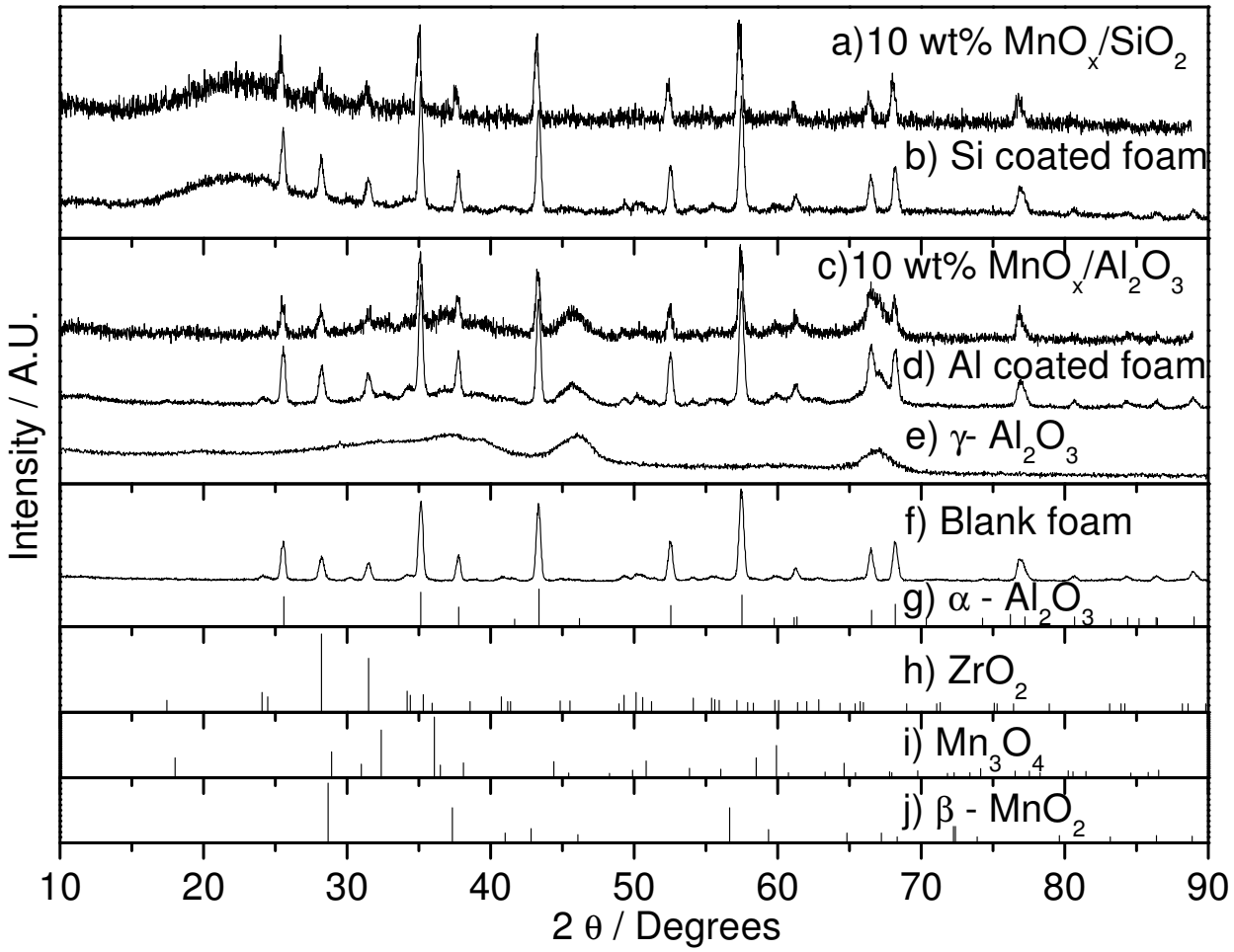

Figure 2-3. XRD traces: a) 10 wt % MnO_x/SiO_2, b) Si coated foam, c) 10 wt % MnO_x/Al_2O_3, d) Al coated foam, e) γ-Al_2O_3, f) blank foam, g) α-Al_2O_3 (PDF 10-173), h) ZrO_2 (PDF 24-1165), i) Mn_3O_4 (PDF 800382), and j) β-MnO_2 (PDF 24-0735).

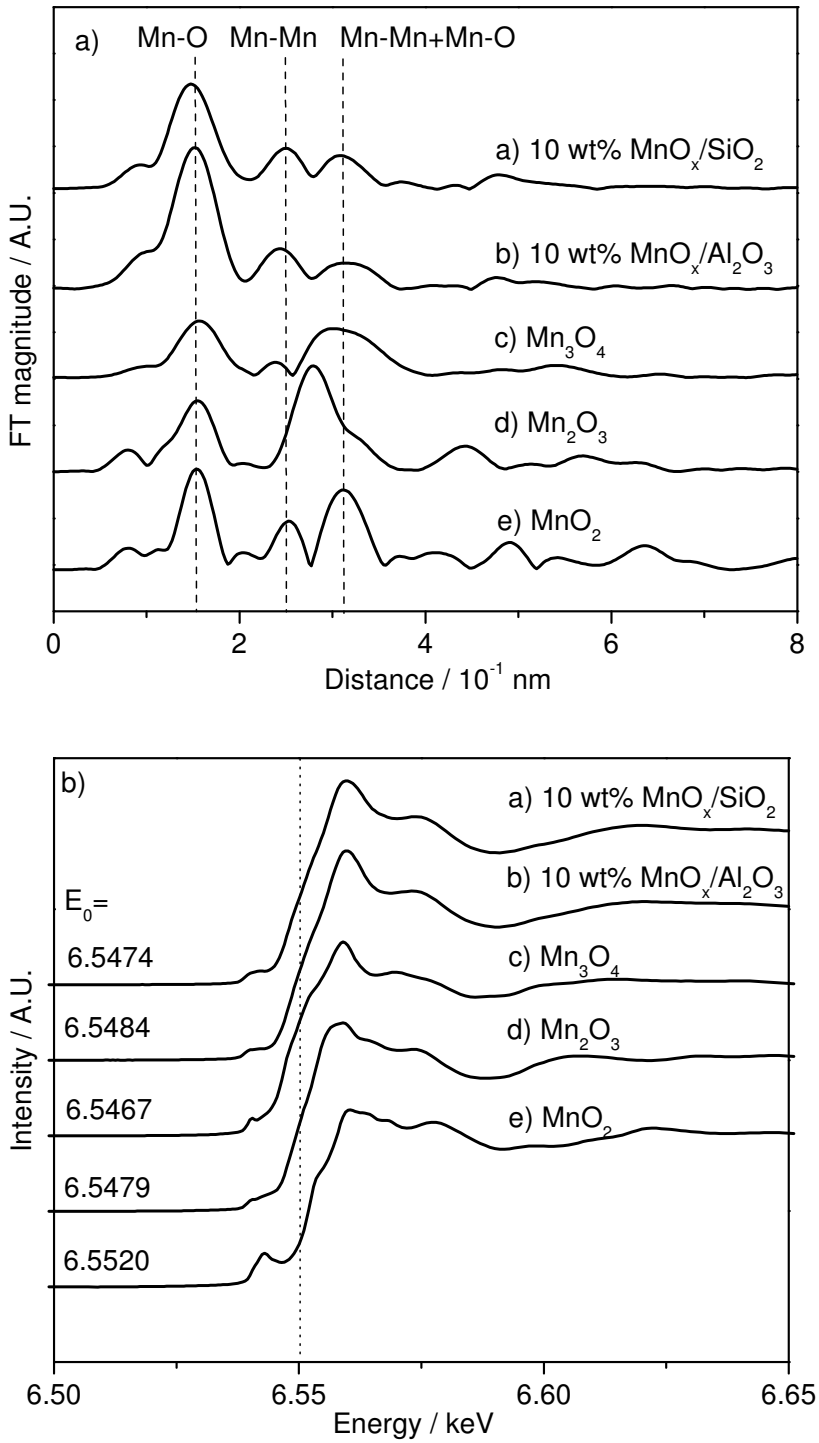

Figure 2-4. a) Fourier transforms of the Mn K-edge EXAFS spectra and b) Mn K-edge XANES spectra: a) 10 wt % MnO_x/SiO_2, b) 10 wt % MnO_x/Al_2O_3, c) Mn_3O_4, d) Mn_2O_3, and e) MnO_2.

Figure 2-5 shows the H_2O^+ (m/e = 18) TPR traces for the 10 wt % MnO_x/SiO_2 and the10 wt % MnO_x/Al_2O_3 foam catalysts. For both samples the traces show an initial reduction peak of manganese oxide at around 493 K and a second reduction peak at around 571 K. They also both have the same onset reduction temperature (T_{red} = 443 K). For the Al_2O_3-supported sample, there is a small feature at low temperature (< 373 K), which may be due to adsorbed water.

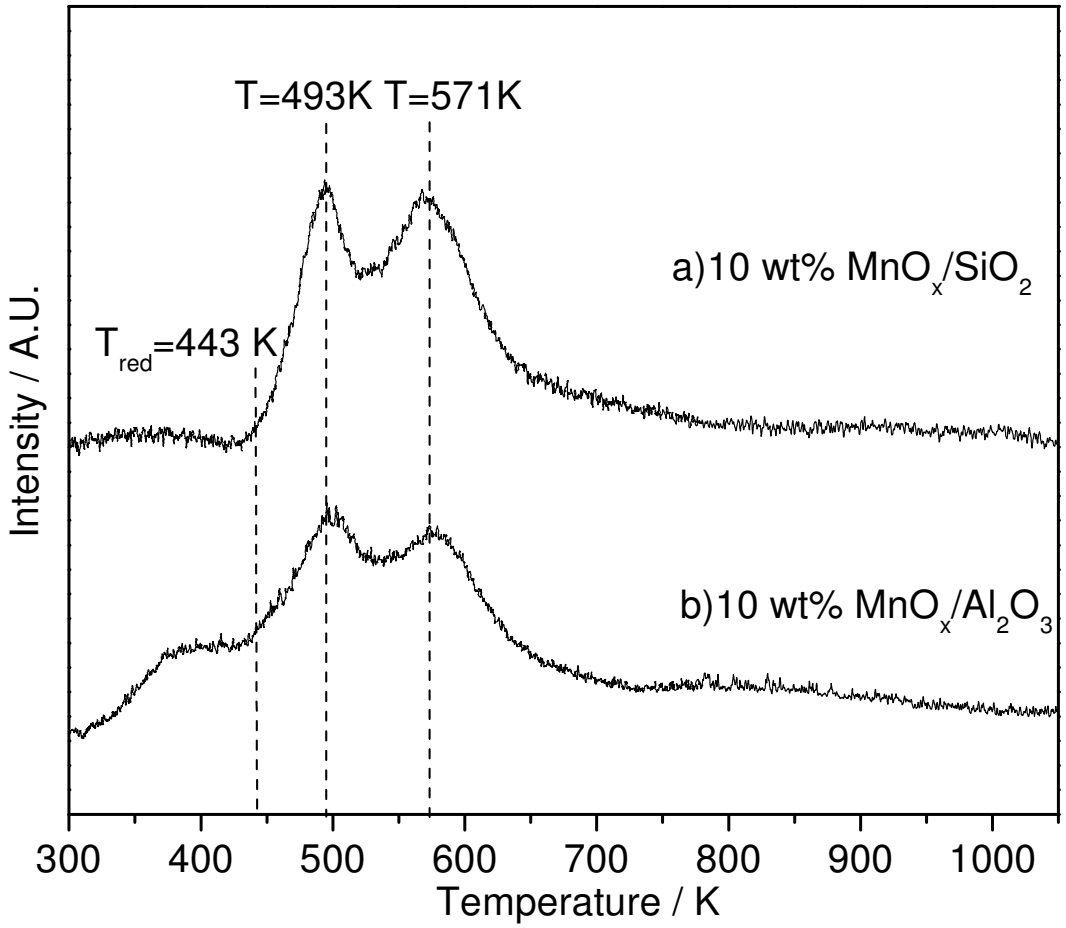

Figure 2-5. TPR traces (m/e = 18) for a) 10 wt % MnO_x/SiO_2 and b) 10 wt % MnO_x/Al_2O_3.

Oxygen uptake and dispersion values for the two catalysts (10 wt % MnO_x/SiO_2 and 10 wt % MnO_x/Al_2O_3) along with the corresponding surface area results based on the overall sample weight and the weight of the washcoat are summarized in Table 2-2. The surface areas of the washcoated foams, a blank foam, and the two supports are also reported.

Table 2-2. Surface area, oxygen chemisorption, and dispersion values.

Catalyst	T_{red} K	S.A. m^2 (g sample)$^{-1}$	S.A. m^2 (g washcoat)$^{-1}$	O_2 Uptake µmol (g sample)$^{-1}$	O_2 Uptake µmol (g washcoat)$^{-1}$	Dispersion %
10 wt% MnO_x/SiO_2	443	21	250	7.3	87	7.2
10 wt% MnO_x/Al_2O_3	443	23	130	3.9	22	6.3
10 wt% MnO_x/SiO_2-H	-	320	-	49	-	-
Al coated foam	-	39	390	-	-	-
Si coated foam	-	61	810	-	-	-
Foam	-	5.0	-	-	-	-
Al_2O_3	-	96	-	-	-	-
SiO_2	-	130	-	-	-	-

2.3.2 Reactivity results

Three series of experiments were performed on the 10 wt % MnO_x/SiO_2 catalyst, 10 wt % MnO_x/Al_2O_3 catalyst, and the blank alumina foam: a) acetone oxidation using an ozone/oxygen mixture, b) acetone oxidation using oxygen alone, and c) ozone decomposition.

The total flow rate was kept at 3.1 L/min (space velocity = 15,000 h^{-1}) except in experiments where the space velocity was varied. The acetone oxidation studies were carried out with a fixed acetone concentration of 0.10 mol % (1,000 ppm) and varying ozone concentrations

of 0-0.80 mol % (0-8,000 ppm) corresponding to ozone/acetone molar ratios (R) ranging from 0 to 8. Catalyst activity was studied as a function of temperature ranging from room temperature to 573 K. The ozone concentration for the reactions presented in Figures 2-6 and 2-7 was 5,000 ppm corresponding to an ozone/acetone molar ratio of 5. In the oxidation reactions CO_2 was the only carbon-containing product observed. The turnover frequencies (TOFs) were calculated for both acetone and ozone conversion using the oxygen uptake values from the oxygen chemisorption experiments and the conversion values.

The effect of temperature on acetone conversion and TOFs are presented in Figure 2-6. Blank acetone oxidation reactions were carried out over the alumina foam with and without ozone. With just air the acetone conversion was less than 10 % even above 550 K. With ozone present acetone reacted at temperatures higher than 450 K but at much lower conversion than with the catalysts present. The conversion of acetone for the reaction with air over the 10 wt % MnO_x/Al_2O_3 and 10 wt % MnO_x/SiO_2 catalysts are shown in Figure 2-6a), which indicates that acetone reacts with oxygen at temperatures higher than 450 K over both catalysts. The conversion of acetone for the reaction with ozone over the 10 wt % MnO_x/Al_2O_3 and 10 wt % MnO_x/SiO_2 catalysts are also shown in Figure 2-6a). It is clear that acetone reacts with ozone already at room temperature. Figure 2-6b) shows the corresponding TOFs for acetone over the two catalysts.

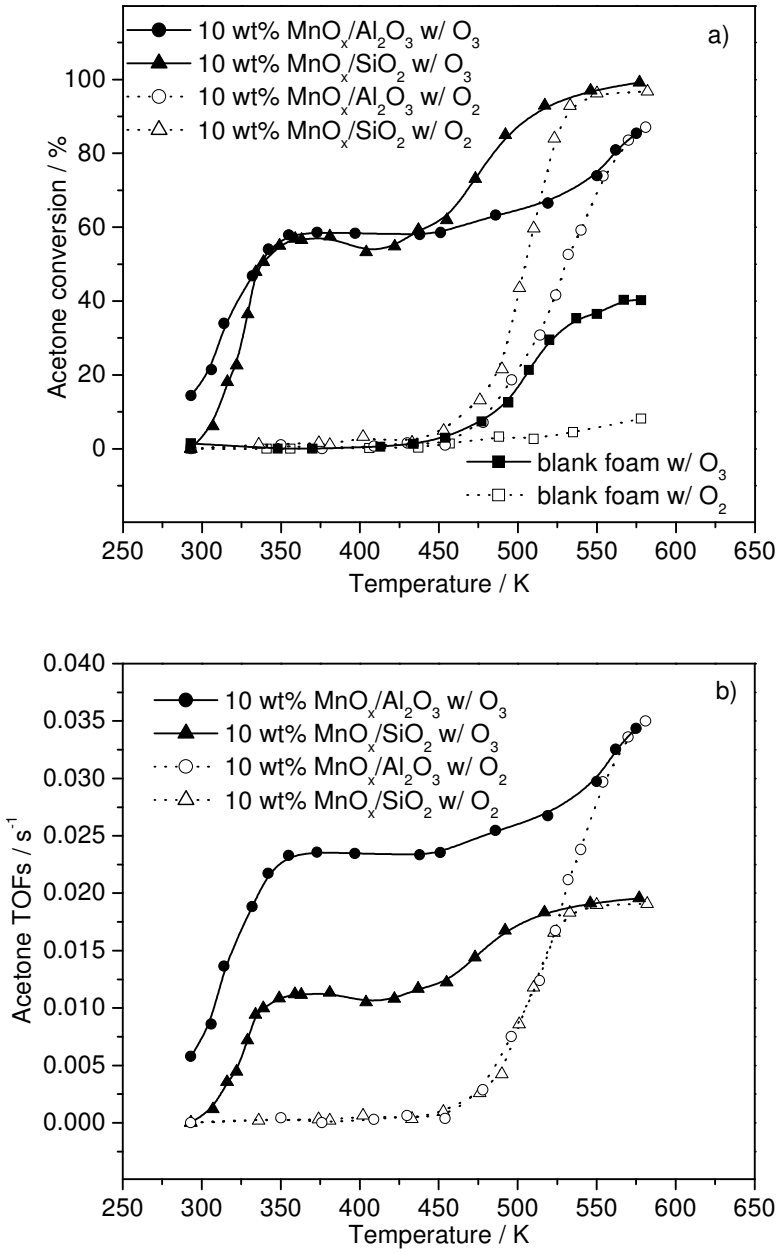

Figure 2-6. a) Acetone conversion versus temperature, and b) TOFs versus temperature for the 10 wt % MnO_x/SiO_2 , 10 wt % MnO_x/Al_2O_3 catalysts, and blank foam in the presence and absence of ozone: (□) blank foam without ozone; (■) blank foam with ozone; (Δ)10 wt % MnO_x/SiO_2 without ozone; (○)10 wt % MnO_x/Al_2O_3 without ozone; (▲)10 wt % MnO_x/SiO_2 with ozone; (●)10 wt % MnO_x/Al_2O_3 with ozone. F_{tot} = 3.1 L/min, S. V. = 15,000 h^{-1}, acetone concentration = 1,000 ppm, ozone concentration = 5,000 ppm.

The effect of temperature on ozone decomposition conversion and TOFs are shown in Figure 2-7. Again, blank reactions of ozone decomposition over the alumina foam with and without acetone were performed and the results are shown in Figure 2-7a). On the foam substrate ozone decomposed at temperatures higher than 350 K without acetone and at temperatures higher than 450 K with acetone. Ozone conversions over the 10 wt % MnO_x/Al_2O_3 and 10 wt % MnO_x/SiO_2 catalysts with and without acetone are shown in Figure 2-7a). The figure shows that ozone starts to decompose from room temperature and is totally decomposed at temperatures higher than 350 K for the 10 wt % MnO_x/SiO_2 catalyst and higher than 400 K for the 10 wt % MnO_x/Al_2O_3 catalyst. The corresponding TOFs of ozone decomposition over the two catalysts are presented in Figure 2-7b).

Figure 2-8 shows the effect of ozone concentration on acetone conversion on the a) 10 wt % MnO_x/SiO_2 and b) 10 wt % MnO_x/Al_2O_3 catalysts. In these reactions the ozone/acetone molar ratio were varied and ranged from 0 to 8, and the conversion of acetone increased with increasing ozone concentration. An acetone conversion around 70 % was obtained using an ozone/acetone molar ratio of 8 at 350 K on both catalysts.

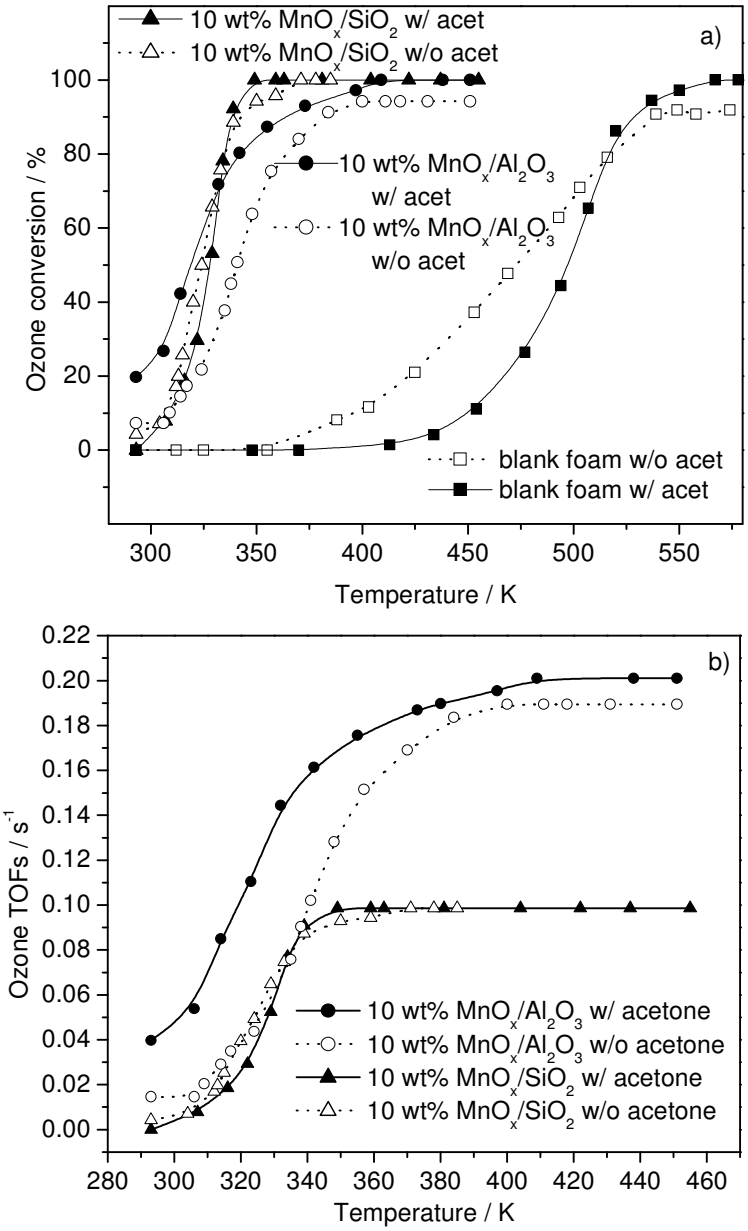

Figure 2-7. a) Ozone conversion versus temperature, and b) TOFs versus temperature for the 10 wt % MnO_x/SiO_2 , 10 wt % MnO_x/Al_2O_3 catalysts, and blank foam in the presence and absence of acetone: (■) blank foam with acetone; (□) blank foam without acetone; (○)10 wt % MnO_x/Al_2O_3 without acetone; (●) 10 wt % MnO_x/Al_2O_3 with acetone; (Δ)10 wt % MnO_x/SiO_2 without acetone; (▲)10 wt % MnO_x/SiO_2 with acetone. F_{tot} = 3.1 L/min, S. V. = 15,000 h^{-1}, acetone concentration = 1,000 ppm, ozone concentration = 5,000 ppm.

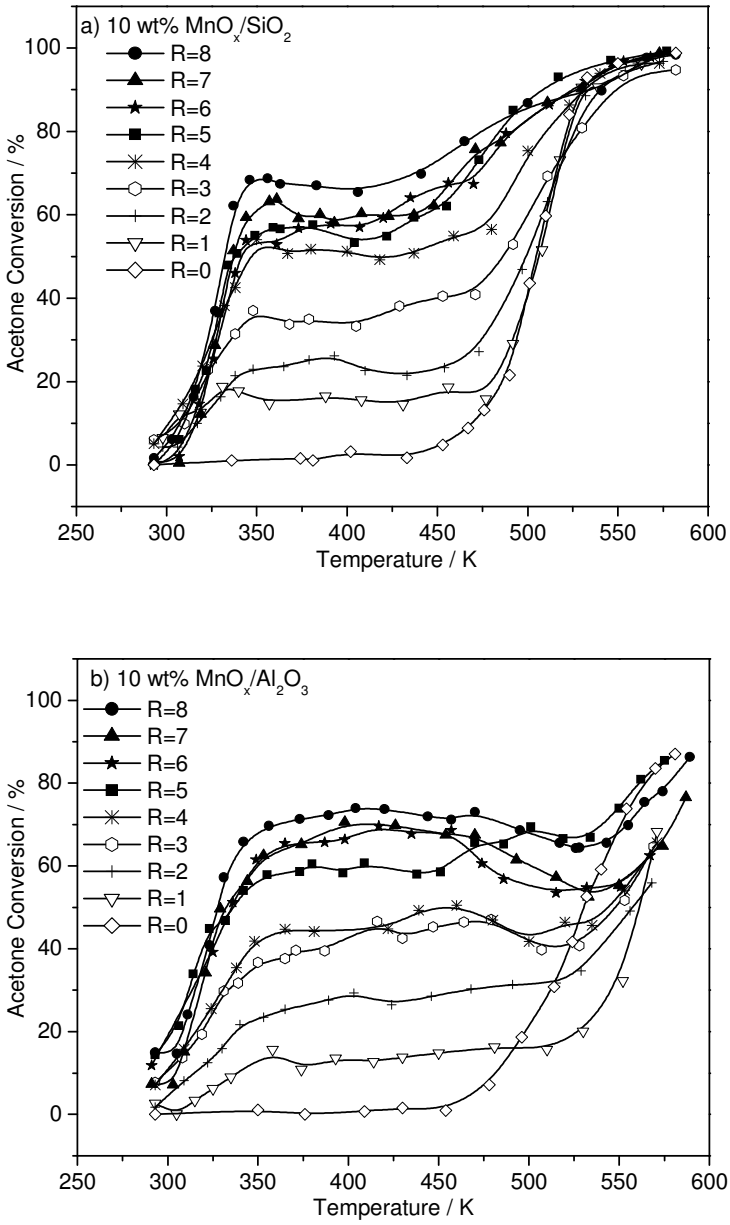

Figure 2-8. Acetone conversion versus temperature for 10 wt % MnO_x/SiO_2 and 10 wt % MnO_x/Al_2O_3 catalysts with various ozone concentrations: a) 10 wt % MnO_x/SiO_2; b) 10 wt % MnO_x/Al_2O_3. R is the ozone/acetone molar ratio. F_{tot} = 3.1 L/min, S. V. = 15,000 h^{-1}, acetone concentration = 1,000 ppm, ozone concentration = 1,000-8,000 ppm.

The effect of space velocity on acetone and ozone conversion as well as pressure drop was also tested over the silica-supported catalyst. In these reactions, the acetone concentration was again 1,000 ppm, the ozone concentration was 5,000 ppm, and the reaction temperature was 325 K. The space velocity varied from 10,000 h^{-1} to 30,000 h^{-1} corresponding to total flow rates ranging from 2.1 L/min to 6.3 L/min. Figure 2-9a) shows the effect of space velocity on the acetone reaction with ozone over the silica-supported catalyst, and Figure 2-9b) shows the effect of space velocity on pressure drop. The conversion of acetone and ozone increased with decreasing space velocity, and the pressure drop increased with increasing space velocity. Figure 2-9b) also displays the theoretical results calculated from the Ergun equation for ceramic foams [12]:

$$\Delta P = \frac{\mu L}{k_1} v_s + \frac{\rho L}{k_2} v_s^2, \tag{3}$$

$$k_1 = \frac{\varepsilon^3 d_p^2}{150(1-\varepsilon)^2}, \tag{4}$$

$$k_2 = \frac{\varepsilon^3 d_p}{1.75(1-\varepsilon)}, \tag{5}$$

where μ is the viscosity of the fluid (for air at 325 K, $\mu = 1.95 \times 10^{-5}$ N s/m^2), ρ is the density of the fluid (for air at 325 K, $\rho = 1.09$ kg/m^3), v_s is the average fluid velocity (internal velocity through the foam), L is the height of the fixed bed (for the foam in this study, $L = 1.3$ cm), d_p is the diameter of the particles in the bed, and ε is the void fraction. For ceramic foams d_p can be defined as

$$d_p = 1.5\frac{(1-\varepsilon)}{\varepsilon} d_c, \tag{6}$$

where d_c is the diameter of the pore in the foam [12]. The foam of 30 ppi pore density has a corresponding d_c of 0.085 cm, the void fraction of the silica-coated foam is approximately 0.56 calculated from the Ergun equation through nonlinear regression fitting using Polymath 5.0 software.

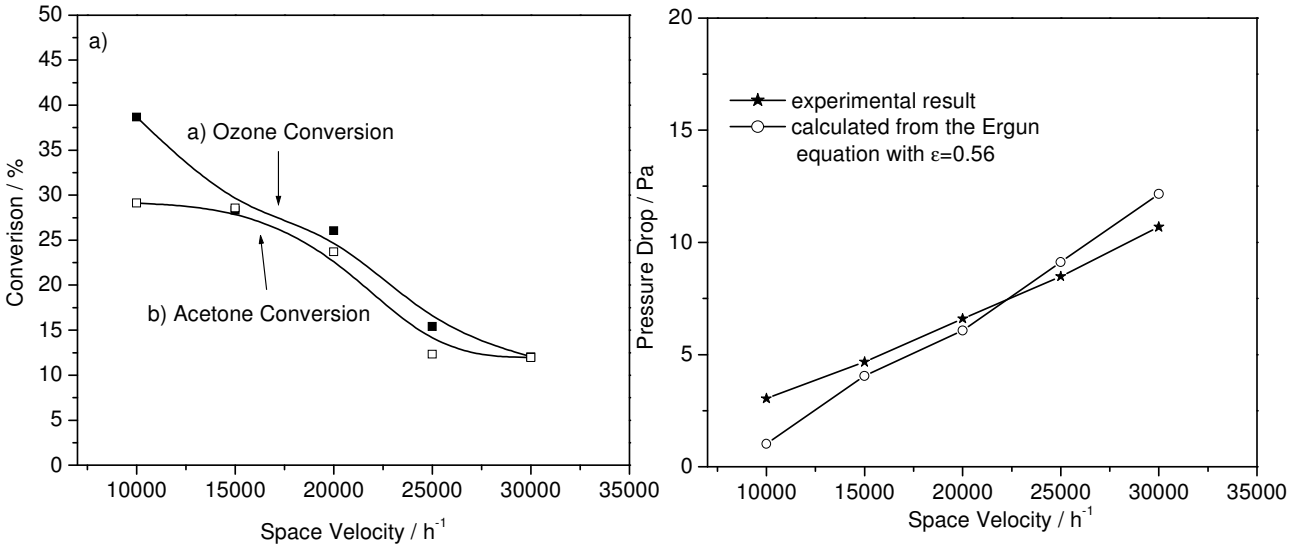

Figure 2-9. a) Acetone and ozone conversion versus space velocity over 10 wt % MnO_x/SiO_2 at temperature 325 K; b) Pressure drop versus space velocity over 10 wt % MnO_x/SiO_2 at temperature 325 K, theoretical results calculated from the Ergun equation at different void fraction (ε). acetone concentration = 1,000 ppm; ozone concentration = 8,000 ppm; space velocity = 10,000 h^{-1} ~ 30,000 h^{-1} corresponding to F_{tot} = 2.1~ 6.3 L/min.

2.3.3 Raman Spectroscopy results

Steady-state, *in situ* Raman spectroscopy results on the 10 wt % MnO_x/SiO_2-H catalyst are presented in Figure 2-10, 2-11, and 2-12. The measurements were successful in characterizing the active phase on the catalyst and identifying two adsorbates on the catalyst surface derived from ozone and acetone. This sample was chosen because it had a high enough surface area to give a significant signal for the adsorbates while maintaining high dispersion.

Figure 2-10 shows the Raman spectra of the 10 wt % MnO_x/SiO_2-H catalyst at different reaction conditions. Figure 2-10a) displays the spectrum of a clean catalyst surface with only oxygen (35 mol %) and helium flowing over the sample, and shows there is a broad peak in the range of 640 – 650 cm^{-1}. Figure 2-10b) displays the spectrum of the catalyst when acetone was included in the gas mixture (0.2 mol % acetone, 35 mol % O_2), and shows there is a peak at 2930 cm^{-1}. Figure 2-10c) displays the spectrum of the catalyst surface when only ozone was added to the initial oxygen/helium mixture (1.0 mol % O_3, 34 mol % O_2), and shows a large peak at 890 cm^{-1} and two other peaks at 1760 cm^{-1} and 2630 cm^{-1}. Figure 2-10d) displays the spectrum of the catalyst surface under reaction conditions when both acetone and ozone were introduced to the sample simultaneously (0.2 mol % acetone, 1.0 mol % O_3, 34 mol % O_2), and shows that the band associated with the ozone significantly diminished in intensity when acetone and ozone were both in the reaction mixture.

Figure 2-11 shows the effect of temperature on the acetone adsorption signal at steady-state without the addition of ozone in the feed stream. As shown, the intensity of the adsorbed acetone peak at 2930 cm^{-1} decreased with increasing temperature.

Figure 2-12 shows the effect of temperature when both acetone and ozone were included in the feed stream. Again, there was a decrease in the intensity of the adsorbed acetone peak

with increasing temperature, but the same trend was not observed for the peak at 890 cm^{-1} associated with ozone. The peak associated with ozone actually increased slightly with increasing temperature.

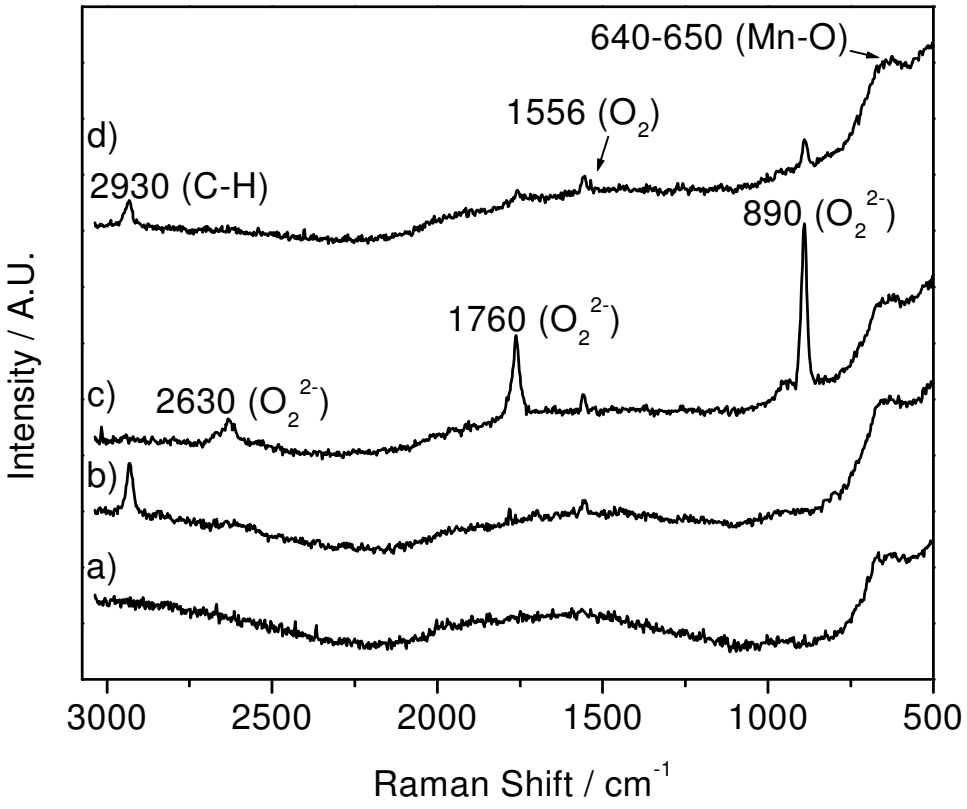

Figure 2-10. Raman spectra of the 10 wt % MnO_x/SiO_2-H exposed to different gas mixtures: a) O_2/He, b) acetone/O_2/He, c) O_3/O_2/He, and d) acetone/O_3/O_2/He.

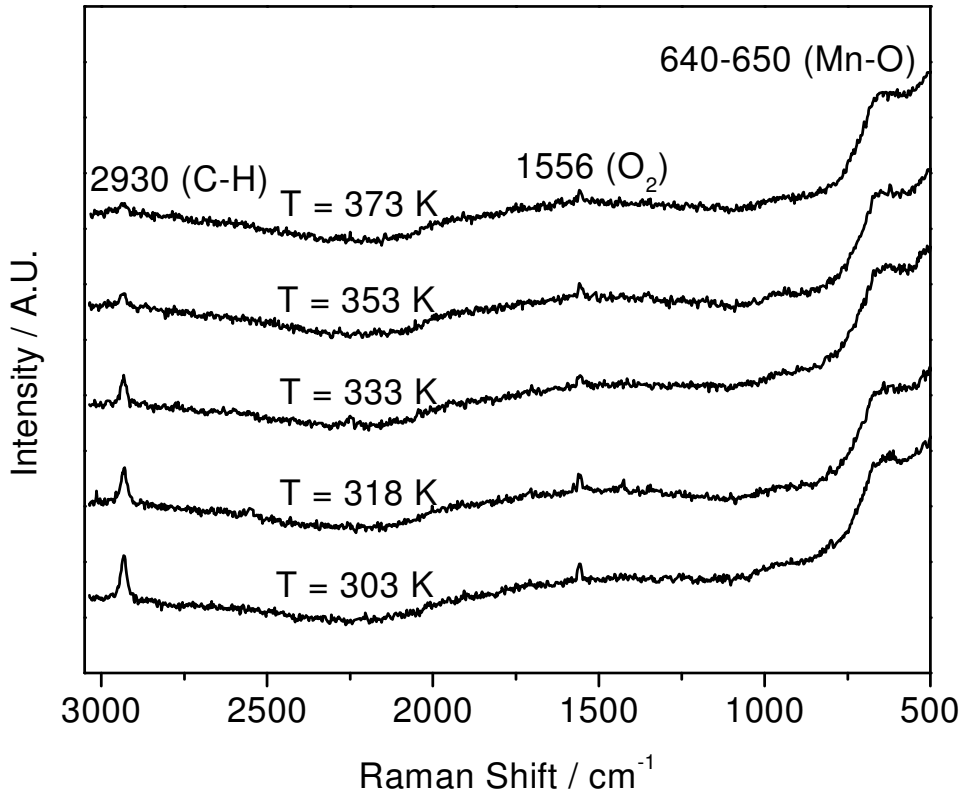

Figure 2-11. Effect of temperature on the 10 wt % MnO_x/SiO_2-H catalyst in acetone/O_2/He.

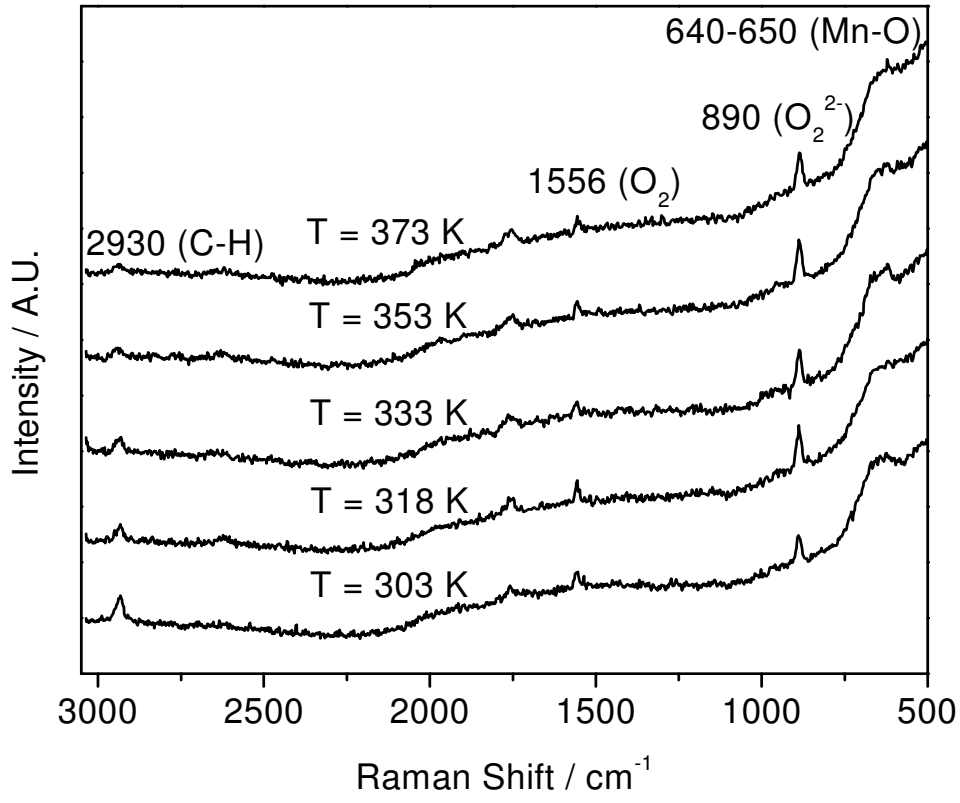

Figure 2-12. Effect of temperature on the 10 wt % MnO_x/SiO_2-H catalyst in acetone/O_3/O_2/He.

2.4 Discussion

2.4.1 Identification of the structure of the supported manganese oxide

The XRD analysis of the foam-supported catalysts indicates that the main phase is α-Al_2O_3 with a ZrO_2 component. No discernable peaks due to manganese oxide are visible in the XRD profiles indicating that the active phase is well dispersed. The TPR profiles were similar

for the two catalysts with two reduction peaks at 493 K and 571 K indicating the presence of similar oxide phases of manganese. They both have the same onset reduction temperature (T_{red} = 443 K).

Because of the lack of XRD features EXAFS spectroscopy was employed to obtain local structure information for the samples. The Fourier transform profiles of the Mn K-edge EXAFS spectra for those samples give three distinctive peaks at 0.15 nm, 0.25 nm, and 0.32 nm. The peaks are close to the respective Mn-O and Mn-Mn distances in both Mn_3O_4 and MnO_2, but cannot be unequivocally assigned to a particular phase because of the similarity in the distances. The XANES spectra of the samples show that the E_0 position for the silica-supported sample is close to that of the Mn_3O_4, and the E_0 position for the alumina-supported sample is close to that of the Mn_2O_3. In another study where silica-supported manganese oxide catalysts of different loadings (3, 10, 15, and 20 wt %) were studied [13], it was found that with lower loading the oxidation state of the samples was close to Mn_2O_3 while with higher loading the oxidation state was close to Mn_3O_4.

2.4.2 Reactivity study

As expected, ozone was a stronger oxidant than oxygen for acetone over both catalysts (Figure 2-6a) and b)). In general, this is in agreement with the results presented by others. Hutchings et al. [14] found that ozone was a more active oxidant than oxygen for methane oxidation over an alumina-supported magnesium catalyst. For both the silica- and alumina-supported catalysts the presence of ozone allowed the oxidation of acetone to occur at close to room temperature with the alumina-supported catalyst showing higher activity. On both catalysts the reaction with oxygen began at substantially higher temperatures (475-500 K). Over

a blank alumina foam acetone did not react with oxygen but did react with ozone in the gas phase at temperatures higher than 450 K (Figure 2-6a)). The gas phase reaction of ozone with organic compounds has been well discussed [15, 16, 17, 18]. Paulis et al. [19] reported a similar phenomenon when they studied the complete oxidation of VOCs, including acetone, over supported manganese oxide catalysts. They found that alumina-supported manganese oxide was more active than silica-supported manganese oxide with the same dispersion. At high temperatures (> 425 K) the acetone conversion increased significantly due to the reaction between oxygen and acetone.

Both the SiO_2- and Al_2O_3-supported catalysts were active in the decomposition of ozone. Figure 2-7a) and b) show that ozone decomposed rapidly over the two catalysts at low temperatures (< 400 K) and reached complete conversion at 350 K over the MnO_x/SiO_2 catalyst and at 400 K over the MnO_x/Al_2O_3 catalyst. The thermal decomposition on the blank foam began only between 400-450 K and was complete at close to 550 K.

The behavior of the catalysts in the presence of ozone was peculiar (Figure 2-6) but can be understood. In both cases the conversions of acetone reached a plateau at about 350 K to further increase above 450 K and join the conversion curves for the reaction with oxygen. The convergence with the oxygen results is expected, since at high temperatures ozone is thermally decomposed and the predominant catalytic pathway is the combustion of acetone with oxygen. The plateau is found exactly at the point (350 K) where ozone conversion is essentially complete. The plateau arises because the acetone reaction at this point is limited by the delivery of oxygen equivalents and the conversion does not rise.

The results in Figure 2-8 with different ozone/acetone ratios (R) can be readily understood from the previous discussion. The figure shows that as the ozone to acetone ratio is

increased, the conversion of acetone increases while at the same time the breadth of the plateau decreases. Both results are due to the increased availability of oxygen equivalents for the oxidation of acetone. For the alumina-supported catalyst the conversion towards the end of the plateau actually dips before rising again. This occurs on this catalyst because the reaction region extends to higher temperatures than for the silica-supported catalyst where ozone starts decomposing thermally. The conversion rises again at the highest temperatures because the reaction of acetone in that region occurs with oxygen from molecular oxygen.

As expected, the pressure drop on the foam catalyst was low and increased with increasing space velocity (Figure 2-9b)). This is in agreement with the results reported by Dhandapani et al. [10], that a foam or monolith gave a smaller pressure drop than pellets with the same surface area. It was reported that a SiC-Al_2O_3 foam containing 50 wt % alumina with a pore density of 30 ppi had a void fraction of 0.89 [12]. But in our results a void fraction of 0.56 was obtained through the theoretical fitting from the Ergun equation. This void fraction is smaller than the reported one probably due to the coverage of the pores with the washcoats. The small pressure drop indicates that foams are promising supports for applications that require high space velocity.

2.4.3 Raman spectra

Figure 2-10 shows that all the spectra of the samples have a broad peak in the range of 640 – 650 cm^{-1}. This peak is assigned as a manganese oxide mode [20], but the identification of the exact phase using Raman spectroscopy is difficult due to the similarity in the Raman modes for the various manganese oxide phases in that range. One study summarized the findings of many Raman studies on bulk manganese oxides and reported that β-MnO_2, α-Mn_2O_3, and Mn_3O_4 all have frequencies in the 640-650 cm^{-1} range [21]. The same study identified the Raman peak

located at ~650 cm^{-1} as characteristic of Mn_3O_4, the most Raman active phase of all manganese oxides. The study concluded that the Raman modes found in this range for the MnO_2 and Mn_2O_3 samples could actually be attributed to Mn_3O_4 formed due to the local heating of the samples during spectrum acquisition. Assuming that there was no local heating due to sample rotation in our experiments, Raman spectroscopy provided further evidence to the XRD and EXAFS analysis presented in another study [13] that the most active phase in this catalyst was similar to Mn_3O_4.

The presence of acetone resulted in a peak at 2930 cm^{-1} (C-H mode) that can be attributed to an adsorbed acetone species (Figure 2-10b). The CH_3 symmetric stretching mode for gas-phase acetone appears at ~2937 cm^{-1} [22]. Also shown in this particular spectrum is a small peak at 1556 cm^{-1}, which is due to gas-phase oxygen. Since the focal point of the collection lens was at the laser spot on the surface of the catalyst sample, the intensity of peaks due to gas-phase species was expected to be weak. This is confirmed by the small signal for the gas-phase oxygen, which is actually in great excess (~1,500 %) over the adsorbed species attributed to ozone. With the presence of ozone there is a large peak at 890 cm^{-1} (Figure 2-10c) which was identified in previous work done in our laboratory to be due to a peroxide species (O-O band) [23, 24]. The features located at 1760 cm^{-1} and 2630 cm^{-1} were overtone bands of the 890 cm^{-1} peak. When both acetone and ozone were introduced to the sample simultaneously the intensity of the peak for ozone was significantly reduced whereas the intensity of the peak due to acetone was hardly affected. This indicates that acetone competes with ozone for active catalyst sites, but that its adsorption is equilibrated. Further evidence shows that acetone adsorption is equilibrated is that the same coverage is obtained regardless of whether the temperature is approached from higher or lower values.

2.4.4 Mechanism of reaction

Comparison of Figure 2-6b) and Figure 2-7b) shows that in the acetone oxidation reaction the TOF of ozone decomposition (0.1-0.2 s^{-1}, maximum) is about 10× larger than the TOF of acetone oxidation (0.01-0.03 s^{-1}, maximum). The stoichiometry of acetone oxidation assuming only one active oxygen per ozone molecule is used (maximum ozone consumption) is

$$CH_3COCH_3 + 8\ O_3 \rightarrow 3CO_2 + 3\ H_2O + 8\ O_2, \quad (7)$$

Thus, about 25 % more ozone is utilized than needed for the oxidation reaction and it is concluded that ozone decomposition occurs in parallel with oxidation.

The relative rates of decomposition of ozone and reaction of ozone with acetone differed on both catalysts. On the 10 wt % MnO_x/Al_2O_3 the rate of reaction of ozone with acetone was higher than the rate of decomposition, while on the 10 wt % MnO_x/SiO_2 the decomposition rate of ozone was slightly higher than the oxidation rate (Figure 2-7b). This indicates that some of the steps in the reaction sequence occurred at different rates on the catalysts.

The following reaction sequence may be used to understand the behavior of the catalysts. The sequence is presented without proof and there may be other possible steps in the actual mechanism. However, as will be discussed below, several parts of the sequence have been verified separately.

$$O_3 + * \quad \rightarrow \quad O_2 + O^*, \quad (8)$$

$$O_3 + O^* \quad \rightarrow \quad O_2 + O_2^*, \quad (9)$$

$$O_2^* \quad \rightarrow \quad O_2 + *, \quad (10)$$

$$CH_3COCH_3 + * \rightarrow CH_3COCH_3*, \quad (11)$$

$$CH_3COCH_3* + O_2* \text{or } O* \rightarrow CO_2 + *, \quad (12)$$

In the sequence the symbol * denotes surface species, including empty sites.

The first three steps are well established for the decomposition of ozone on manganese oxide catalysts from kinetic, spectroscopic, isotopic, and computational studies [23, 24, 25, 26]. The inclusion of these steps reflects the observation that ozone decomposition occurs in parallel with the oxidation of acetone. The fourth step is evidenced by *in situ* Raman studies of acetone oxidation with ozone (Figure 2-10a), which show the presence of an adsorbed species with intact C-H bonds whose surface concentration is little affected by the presence of ozone. The last step starts a sequence of oxidation steps that leads to full oxidation and reflects the findings that there are no other adsorbed species observed and that CO_2 is the only carbon-containing product of the oxidation. The complete, facile oxidation of the adsorbed acetone once it is attacked by a reactive oxygen species is reasonable, as the molecule becomes activated to further reaction.

A question that remains open is whether the oxidizing species is atomic (O*) or molecular (O_2*). In ozone decomposition the most abundant surface species is the peroxidic, molecular form, which is readily observed by *in situ* Raman spectroscopy [23, 24, 25, 26], and this indicates that its decomposition through reaction (10) is a slow step. It is likely though, at least for the alumina-supported catalyst, that the reactive intermediate for acetone oxidation is the atomic form. The reason is the observation that the overall rate of the ozone decomposition reaction is faster in the presence of acetone. This is unexpected, as the adsorbed acetone competes for sites, and would be expected to retard the reaction. This can be seen from the Raman spectra results in Figure 2-10d which showed that acetone significantly reduced the

coverage by the peroxide species derived from ozone. However, if the acetone acts as a sink for the oxygen atoms, it could accelerate the usage of ozone by freeing up empty sites. The reaction of the oxygen atoms would reduce the concentration of the peroxide intermediates as observed.

2.5 Conclusions

XRD and EXAFS spectroscopies were used to characterize the structure of the catalysts. No discernable peaks due to manganese oxide are visible in the XRD profiles indicating that the active phase is well dispersed. The Fourier transform profiles of the Mn K-edge EXAFS spectra for those samples gave three distinctive peaks at 0.15 nm, 0.25 nm, and 0.32 nm and were close to the profiles of Mn_3O_4 and MnO_2. The TPR traces for both catalysts were similar, with two reduction peaks at 493 K and 571 K indicating the presence of similar metal oxide phases for both catalysts. The same onset reduction temperature (T_{red} = 443 K) was also obtained for both catalysts. The number of surface active sites was determined through oxygen chemisorption measurements at this temperature, and it was found that the silica-supported catalyst had a larger atomic oxygen uptake than the alumina-supported catalyst. *In situ* steady-state Raman spectroscopy measurements during acetone catalytic oxidation showed the presence of an adsorbed acetone species with a C-H bond at 2930 cm^{-1} and a peroxide species derived from ozone with a bond at 890 cm^{-1}. It was shown that there was a competition for the active catalyst sites between these two reactants during the reaction. When both acetone and ozone were introduced to the sample simultaneously the intensity of the peak for ozone was significantly diminished whereas the intensity of the peak due to acetone was hardly affected.

Acetone catalytic oxidation using ozone was studied from room temperature to 573 K. The introduction of ozone reduced the reaction temperature on both the alumina- and silica-

supported catalysts. The only carbon-containing product detected in all reactions was CO_2. The alumina-supported catalyst was found to be more active with higher turnover frequencies (TOFs) compared to the silica-supported catalyst in the acetone oxidation and ozone decomposition reactions. The conversion of acetone increased with increasing ozone concentration. With increasing space velocity the conversion of acetone and ozone decreased due to the shorter contact time. For the foam supported catalyst the pressure drop was small and indicates that the foams are promising materials as catalyst supports in high flow rate applications such as air pollution control.

Acknowledgement

Many thanks are due to Corey Reed for the use of the Raman data and discussion, which are part of his dissertation.

References:

(1) A. Gil, N. Burgos, M. Paulis, M. Montes, L. M. Gandía, *Stud. in Surf. Sci. and Catal.*, **2000**, 130, 2153.

(2) K. M. Parida, A. Samal, *Appl. Catal. A*, **1999**, 182, 249.

(3) V. Ragaini, C. L. Bianchi, G. Forcella, A. Gervasini, *Trends in Ecological Physical Chemistry*, Milan, Italy, **1992**, 275.

(4) A. Gervasini, C. L. Binachi, V. Ragaini, In *Environmental catalysis*, J. N. Armor Ed., ACS Symp. Ser. 552; ACS: Washington, DC, **1994**, 352.

(5) M. Baldi, E. Finocchio, F. Milella, G. Busca, *Appl. Catal. B*, **1998**, 16, 43.

(6) T. J. Lu, H. A. Stone, M. F. Ashby, *Acta Metallurg. Inc*., **1998**, 46, 3619.

(7) A. G. Dietz III, A. F. Carlsson, and L. D. Schmidt, *J. Catal*., **1996**, 176, 459.

(8) M. Huff, L. D. Schmidt, *J. Catal*., **1995**, 155, 82.

(9) J. P. DeLuca, L. E. Campbell, In *Monolithic Catalyst Supports, Advanced Materials in Catalysis*, J. J. Burton, R. L. Garten, Eds., Academic Press, New York, **1977**.

(10) B. Dhandapani, S. T. Oyama, *Appl. Catal. B*, **1997**, 11, 129.

(11) F. C. Patcas*, J. Catal*., **2005**, 231, 194.

(12) M. D. M. Innocentini, V. R. Salvini, A. Macedo, V. C. Pandolfelli, *Mat. Res*, Vol. 2, No. 4, **1999**, 283.

(13) C. Reed, Y. Xi, Y-K. Lee, S. T. Oyama, *J. Catal.*, Submitted.

(14) G. J. Hutchings, M. S. Scurrell, J. R. Woodhouse, *Appl. Catal*., **1988**, 38, 157.

(15) P. S. Bailey, *Ozonation in Chemistry*, Academic Press, New York, **1978**, Vol. 1.

(16) P. S. Bailey, *Ozonation in Chemistry*, Academic Press, New York, **1978**, Vol. 2.

(17) R. Atkinson, W. P. L. Carter, *Chem. Rev*., **1987**, 84, 437.

(18) S. T. Oyama, *Catal. Rev. Sci. Eng*., **2000**, 42, 279.

(19) M. Paulis, L. M. Gandía, A. Gil, J. Sambeth, J. A. Odriozola, M. Montes, *Appl. Catal. B*, **2000**, 26, 37.

(20) F. Kapteijn, A. D. van Langeveld, J. A. Moulijn, A. Andreini, M. A. Vuurman, A. M. Turek, J. M. Jehng, I. E. Wachs, *J. Catal*., **1994**, 150, 94.

(21) F. Buciuman, F. Patcas, R. Craciun, D. R. T. Zahn, *Phys. Chem. Chem. Phys.*, **1999**, 1, 185.

(22) NIST Chemistry WebBook, "http://webbook.nist.gov/cgi/cbook.cgi?Name=acetone&Units=SI&cTG=on&cIR=on&cTC=on&cMS=on&cTP=on&cUV=on&cTR=on&cES=on&cIE=on&cDI=on&cIC=on&cSO=on#IR-Spec," 6, April, **2005**.

(23) W. Li, G. V. Gibbs, S. T. Oyama, *J. Am. Chem. Soc*., **1998**, 120, 9041.

(24) W. Li, S. T. Oyama, *J. Am. Chem. Soc*., **1998**, 120, 9047.

(25) R. Radhakrishnan, S. T. Oyama, J. G. Chen, K. Asakura, *J. Phys. Chem. B*, **2001**, 105, 4245.

(26) R. Radhakrishnan, S. T. Oyama, *J. Catal*., **2001**, 199, 282.